Syntaxin 3 is essential for photoreceptor outer segment protein trafficking and survival

Mashal Kakakhel[a], Lars Tebbe[a], Mustafa S. Makia[a], Shannon M. Conley[b,c], David M. Sherry[b,c,d], Muayyad R. Al-Ubaidi[a,e,f,1], and Muna I. Naash[a,e,f,1]

[a]Department of Biomedical Engineering, University of Houston, Houston, TX 77204; [b]Department of Cell Biology, University of Oklahoma Health Sciences Center, Oklahoma City, OK 73104; [c]Oklahoma Center for Neurosciences, University of Oklahoma Health Sciences Center, Oklahoma City, OK 73104; [d]Department of Pharmaceutical Sciences, University of Oklahoma Health Sciences Center, Oklahoma City, OK 73104; [e]College of Optometry, University of Houston, Houston, TX 77204; and [f]Department of Biology and Biochemistry, University of Houston, Houston, TX 77204

Edited by John E. Dowling, Harvard University, Cambridge, MA, and approved July 15, 2020 (received for review May 26, 2020)

Trafficking of photoreceptor membrane proteins from their site of synthesis in the inner segment (IS) to the outer segment (OS) is critical for photoreceptor function and vision. Here we evaluate the role of syntaxin 3 (STX3), in trafficking of OS membrane proteins such as peripherin 2 (PRPH2) and rhodopsin. Photoreceptor-specific *Stx3* knockouts [$Stx3^{f/f(iCre75)}$ and $Stx3^{f/f(CRX\text{-}Cre)}$] exhibited rapid, early-onset photoreceptor degeneration and functional decline characterized by structural defects in IS, OS, and synaptic terminals. Critically, in the absence of STX3, OS proteins such as PRPH2, the PRPH2 binding partner, rod outer segment membrane protein 1 (ROM1), and rhodopsin were mislocalized along the microtubules to the IS, cell body, and synaptic region. We find that the PRPH2 C-terminal domain interacts with STX3 as well as other photoreceptor SNAREs, and our findings indicate that STX3 is an essential part of the trafficking pathway for both disc (rhodopsin) and rim (PRPH2/ROM1) components of the OS.

syntaxin 3 | retinal degeneration | SNAREs | tetraspanin | Prph2

Proper assembly of the photoreceptor outer segment (OS), a modified primary cilium, is essential for vision. The OS is a unique structure consisting of stacks of membranous discs containing the machinery for phototransduction. It also represents a unique challenge for the biosynthetic machinery because the OS discs are constantly shed from the distal tips and renewed from the base (1, 2). Approximately 10% of OS material is turned over every day, thus large quantities of protein and lipid must be constantly synthesized and trafficked to the OS. This process is made even more complicated by the fact that rods and cones have different OS structure and different trafficking as well as by the precise organization of the OS. Newly synthesized proteins must be correctly sorted into either the plasma membrane domain, the disc domain, and/or the disc rim domain. This sophisticated, high-capacity trafficking and sorting system is essential for photoreceptor function but remains poorly understood, despite significant recent advances in the area. Membrane proteins destined for the OS are synthesized and packaged in the inner segment (IS), then delivered to the plasma membrane at the base of the OS. These trafficking vesicles fuse with the plasma membrane, after which proteins transport to the OS via the plasma membrane of the connecting cilium and incorporate into newly evaginating OS discs (3–6).

Peripherin 2 (PRPH2 also known as RDS), is a membrane protein essential for disc rim structure (7, 8). Mutations in *PRPH2* cause various rod- and cone-dominant retinal degenerations in patients (9), and mice lacking PRPH2 do not form OSs (10). Studies suggest that PRPH2 traffics to the OS in different vesicles than other OS components such as rhodopsin or cone opsins (11–15). This idea is underscored by the finding that PRPH2 is trafficked in large part via an unconventional secretory pathway that bypasses the trans-Golgi and may involve the endosomal recycling system (16–19). However, the precise mechanisms that regulate the trafficking of PRPH2 remain unclear. In previous mass spectrometry experiments, we identified and validated PRPH2 interacting partners, including syntaxin 3 (STX3) and SNAP25 (17). STX3 and SNAP25 are members of the soluble NSF attachment protein receptor (SNARE) family. These proteins are involved in vesicle fusion with the photoreceptor plasma membrane and are known to participate in trafficking rhodopsin (20) as well as in synaptic vesicle release. Interestingly, we found that rhodopsin also interacts with STX3 (17), so we hypothesize that STX3-mediated fusion events might be a common mechanism by which vesicles trafficked through both conventional and unconventional secretory pathways converge on the way to the OS.

To evaluate the role of STX3 in trafficking OS disc proteins such as PRPH2 and rhodopsin, we eliminated STX3 in photoreceptors using a conditional knockout mouse line. In the absence of STX3, photoreceptors undergo rapid degeneration and OS proteins including PRPH2, the PRPH2 binding partner ROM1, and rhodopsin are mistrafficked. These findings confirm the importance of STX3 for trafficking of OS disc proteins and significantly enhance our understanding of the essential interplay between IS trafficking and OS structure.

Results

CRX-Cre and iCre75 Lead to Effective Knockdown of STX3 in the Retina. Global knockout of *Stx3* is lethal (21), so we generated a conditional knockout, with LoxP sites flanking exons 4 and 5

Significance

Rod and cone photoreceptors are highly polarized cells which rely on incompletely understood trafficking pathways to deliver and sort proteins into multiple outer segment subcompartments (disc, rim, and plasma membrane). Here we identify the SNARE protein syntaxin 3 as a trafficking component for both disc and rim proteins but not plasma membrane proteins. Our results suggest that syntaxin 3-mediated vesicle fusion is a convergence point for disc and rim protein trafficking and sorting. Furthermore, we find no evidence that eliminating syntaxin 3 affects cone photoreceptor trafficking, suggesting that divergent trafficking pathways in the two cell types may underlie their different outer segment structure. These studies significantly enhance our understanding of the unique and elegant cell biology of the photoreceptor.

Author contributions: M.R.A.-U. and M.I.N. designed research; M.K., L.T., M.S.M., and D.M.S. performed research; M.K., L.T., M.S.M., S.M.C., D.M.S., M.R.A.-U., and M.I.N. analyzed data; and M.K., S.M.C., M.R.A.-U., and M.I.N. wrote the paper.

The authors declare no competing interest.

This article is a PNAS Direct Submission.

[1]To whom correspondence may be addressed. Email: malubaid@central.uh.edu or mnaash@central.uh.edu.

This article contains supporting information online at https://www.pnas.org/lookup/suppl/doi:10.1073/pnas.2010751117/-/DCSupplemental.

First published August 10, 2020.

(*SI Appendix*, Fig. S1) which are required for all four STX3 isoforms (STX3A–D) (22) (*SI Appendix*, Fig. S1*A*). STX3 is the major syntaxin in photoreceptors (23), with STX3B being the only STX3 isoform expressed.

STX3 is expressed throughout postnatal development (*SI Appendix*, Fig. S2*A*), and in the adult retina is distributed in all photoreceptor compartments except the OS (17, 23). To knock down STX3 in specific retinal cells, we used either the cone-rod homeobox (CRX)-Cre (24, 25) or the rhodopsin Cre (iCre75) (26). CRX is initially expressed at embryonic day 12.5 (24, 27, 28) (*SI Appendix*, Fig. S2*B*), and the promoter fragment used to generate the CRX-Cre line generates early knockdown in both rods and cones as well as some bipolar cells (25). The iCre75 promoter leads to Cre activation in rods at approximately postnatal day 9 (P9) (26) (*SI Appendix*, Fig. S2*B*), but is not expressed in cones or other retinal cells. In the $Stx3^{f/f(iCre75)}$ mice, STX3 protein levels in the retina dropped dramatically as Cre levels increased (*SI Appendix*, Fig. S2 *C* and *E*), while in $Stx3^{f/f(CRX\text{-}Cre)}$ retinas, the earlier onset of Cre expression led to low STX3 protein levels from birth (*SI Appendix*, Fig. S2 *D* and *F*). Overall there was 76% knockdown in STX3 levels in $Stx3^{f/f(iCre75)}$ retinas at P30 compared to $Stx3^{f/f}$ littermates (referred to as wild type [WT]), and 94% knockdown in $Stx3^{f/f(CRX\text{-}Cre)}$ retinas at P15 (Fig. 1*B*). As expected, $Stx3^{f/f(iCre75)}$ retinas exhibit no STX3 expression in rods, in contrast to cones and inner retinal cells (Fig. 1 *A* and *C*). In the $Stx3^{f/f(CRX\text{-}Cre)}$, no STX3 was found in photoreceptors (Fig. 1*A*). Consistent with developmental expression of CRX-Cre in bipolar cells (25), little labeling for STX3 was present in the inner retina in the $Stx3^{f/f(CRX\text{-}Cre)}$ (Fig. 1*C*).

Elimination of STX3 Leads to Profound Degeneration and Functional Impairment in the Retina. Significant photoreceptor degeneration was evident by P15 in $Stx3^{f/f(CRX\text{-}Cre)}$ retinas (Fig. 2 *A* and *B*), and no photoreceptors remained by P30 (Fig. 2 *A* and *B*, *Middle* and *SI Appendix*, Fig. S3*B*). Degeneration was slower in $Stx3^{f/f(iCre75)}$ retinas: progressive loss of photoreceptors was observed from P21 to P60 (Fig. 2 *A* and *B* and *SI Appendix*, Fig. S3*A*). The OS layer was also thinner in both $Stx3^{f/f(CRX\text{-}Cre)}$ and $Stx3^{f/f(iCre75)}$ compared to WT (Fig. 2*A*, red bars and *SI Appendix*, Fig. S3), and by P21 no OSs were present in the $Stx3^{f/f(CRX\text{-}Cre)}$ retina. By P45, remaining OSs in the $Stx3^{f/f(iCre75)}$ were extremely short. Inner nuclear layer (INL) thickness was also reduced in the $Stx3^{f/f(CRX\text{-}Cre)}$ retina at P21 (Fig. 2*C*), consistent with STX3 knockout from the inner retina in this line, but was unaffected in $Stx3^{f/f(iCre75)}$ mice (Fig. 2*C*). Heterozygous mice did not exhibit degeneration and were not evaluated further (*SI Appendix*, Fig. S3).

Transmission electron microscopy (TEM) showed that ISs had an abnormal accumulation of vesicles and membranous debris and a rounder, swollen appearance in the $Stx3^{f/f(CRX\text{-}Cre)}$ (Fig. 2 *D*, arrows and *Inset*, P15) and $Stx3^{f/f(iCre75)}$ (Fig. 2*F*, P21) retinas compared to WT. OSs in the $Stx3^{f/f(CRX\text{-}Cre)}$ retina had irregular disc size, stacking, and alignment at P15 (Fig. 2*E*, arrows). At P21, OSs and ISs were rare in the $Stx3^{f/f(CRX\text{-}Cre)}$ retina, and those that remained exhibited severe structural abnormalities (Fig. 2 *F* and *G*, *Insets*). In the P21 $Stx3^{f/f(iCre75)}$, some OSs were largely normal (though shorter than WT), while others exhibited severe abnormalities in disc alignment and sizing, as well as accumulation of debris (Fig. 2*G*, arrows). By P45, $Stx3^{f/f(iCre75)}$ OSs shortened further with significant empty space in the OS layer due to photoreceptor loss (Fig. 2 *H* and *I*).

Connecting cilia existed at ages when OSs were still present [P15 and 19 for $Stx3^{f/f(CRX\text{-}Cre)}$ and P21 and 30 for $Stx3^{f/f(iCre75)}$] though they often appeared swollen (white arrows highlight cilia in Fig. 2*J*). Measurement of the acetylated region of the axoneme was performed and the length of the acetylated region was found to be significantly reduced in $Stx3^{f/f(CRX\text{-}Cre)}$ and $Stx3^{f/f(iCre75)}$ retinas compared to WT (Fig. 2 *K* and *L*) at P15 and P21, respectively.

STX3 is also found at photoreceptor synapses, so we evaluated synaptic structure. WT terminals were normal, showing long synaptic ribbons, synaptic vesicles (Fig. 3*A* and *SI Appendix*, Fig. S4*A*, arrows), and postsynaptic horizontal and bipolar cell processes in rods and cones and flat contacts in cones (arrowheads, Fig. 3*A*). Rods and cones in the $Stx3^{f/f(iCre75)}$ formed ribbon synapses, but showed progressive synaptic pathology, more severe in rods than cones, and were characterized by extensive synaptic ribbon remodeling, and some ribbons appeared to be free floating (at P21, black arrows, Fig. 3*B*, and *SI Appendix*, Fig. S4). Cone terminals from $Stx3^{f/f(iCre75)}$ mice had less synaptic disruption than rod terminals. Cones formed ribbon synapses and flat contacts (black arrowheads, Fig. 3*B*) until at least P45 (*SI Appendix*, Fig. S4*B*), although some synaptic ribbons showed a decline in structural integrity.

Rod and cone terminals in the $Stx3^{f/f(CRX\text{-}Cre)}$ retina showed abnormalities from the earliest time examined, P15 (*SI Appendix*, Fig. S4*C*), and progressive rod terminal loss was followed by cone terminal loss. Many rod terminals showed abnormally small, free floating ribbons (arrows, Fig. 3*C*), no discrete arciform densities, and free-floating presumptive ribbon material. Others lacked visible ribbons and contained abnormal vesicles, vacuoles, and multivesicular bodies, which became more pronounced with age (Fig. 3*C*, * and *SI Appendix*, Fig. S4*C*). Cone terminals also showed abnormalities in the $Stx3^{f/f(CRX\text{-}Cre)}$ retina, but were less affected than rods. There was little evidence of invagination by postsynaptic processes at ribbon contacts in rods or cones, and when present, appeared to originate from horizontal cells rather than bipolar cells (Fig. 3*C*). These findings were confirmed by immunofluorescence (IF) labeling: little colocalization between the rod spherule marker plasma membrane Ca2+ ATPase (PMCA) (29, 30) and the bipolar cell marker protein kinase C (PKC) (Fig. 3*E*) or the horizontal cell marker calbindin (*SI Appendix*, Fig. S5*A*) was observed in terminals in the $Stx3^{f/f(CRX\text{-}Cre)}$. Gross outer plexiform layer (OPL) defects were also visible. In the P15 $Stx3^{f/f(CRX\text{-}Cre)}$, the OPL was thinner than in WT, fewer photoreceptor terminals were present (Fig. 3*D*), and there was increased PMCA labeling within the outer nuclear layer (ONL), a common feature of degenerating photoreceptors, which retract their terminals out of the OPL as they die (Fig. 3 *D* and *E*, arrowheads). However, there was proper stratification of rod bipolar cell terminals (PKC) and VGLUT3 amacrine cell processes suggesting that the inner plexiform layer was undisturbed in $Stx3^{f/f(CRX\text{-}Cre)}$ and $Stx3^{f/f(iCre75)}$ retinas (*SI Appendix*, Fig. S5 *B*–*D*). Together, these results suggest that the absence of STX3 is deleterious to rod and cone synapses, and that rods are more severely affected than cones.

Retinal function measured by full-field electroretinography (ERG) was also reduced in STX3 knockouts. Scotopic (rod-driven) a-wave ERGs were significantly reduced by ~55% at P30 and ~66% at P60 (Fig. 4 *A* and *C*). Scotopic b-waves were similarly reduced, and scotopic a-/b-wave ratios were similar in WT and $Stx3^{f/f(iCre75)}$ mice, consistent with the overall lack of degeneration in the inner retina in the $Stx3^{f/f(iCre75)}$. Photopic (cone-driven) b-wave amplitudes in the $Stx3^{f/f(iCre75)}$ retina did not differ from WT controls at any time point (Fig. 4 *B* and *D*), although oscillatory potentials were reduced (Fig. 4*B*). Preservation of cone function is consistent with rod-specific STX3 knockout in $Stx3^{f/f(iCre75)}$ mice. In keeping with the more severe structural defects in the $Stx3^{f/f(CRX\text{-}Cre)}$ retina, these animals exhibited no scotopic or photopic ERG responses at any time points examined (Fig. 4).

Eliminating STX3 Impairs Photoreceptor OS Protein Trafficking. We examined the localization of the OS proteins PRPH2, the PRPH2 binding partner ROM1, rhodopsin, and cone opsins, at ages when OSs were still present [P21 for $Stx3^{f/f(iCre75)}$ and P15 for $Stx3^{f/f(CRX\text{-}Cre)}$]. PRPH2, ROM1, and rhodopsin are all proteins that interact with STX3 (17). In both knockout lines, a portion of

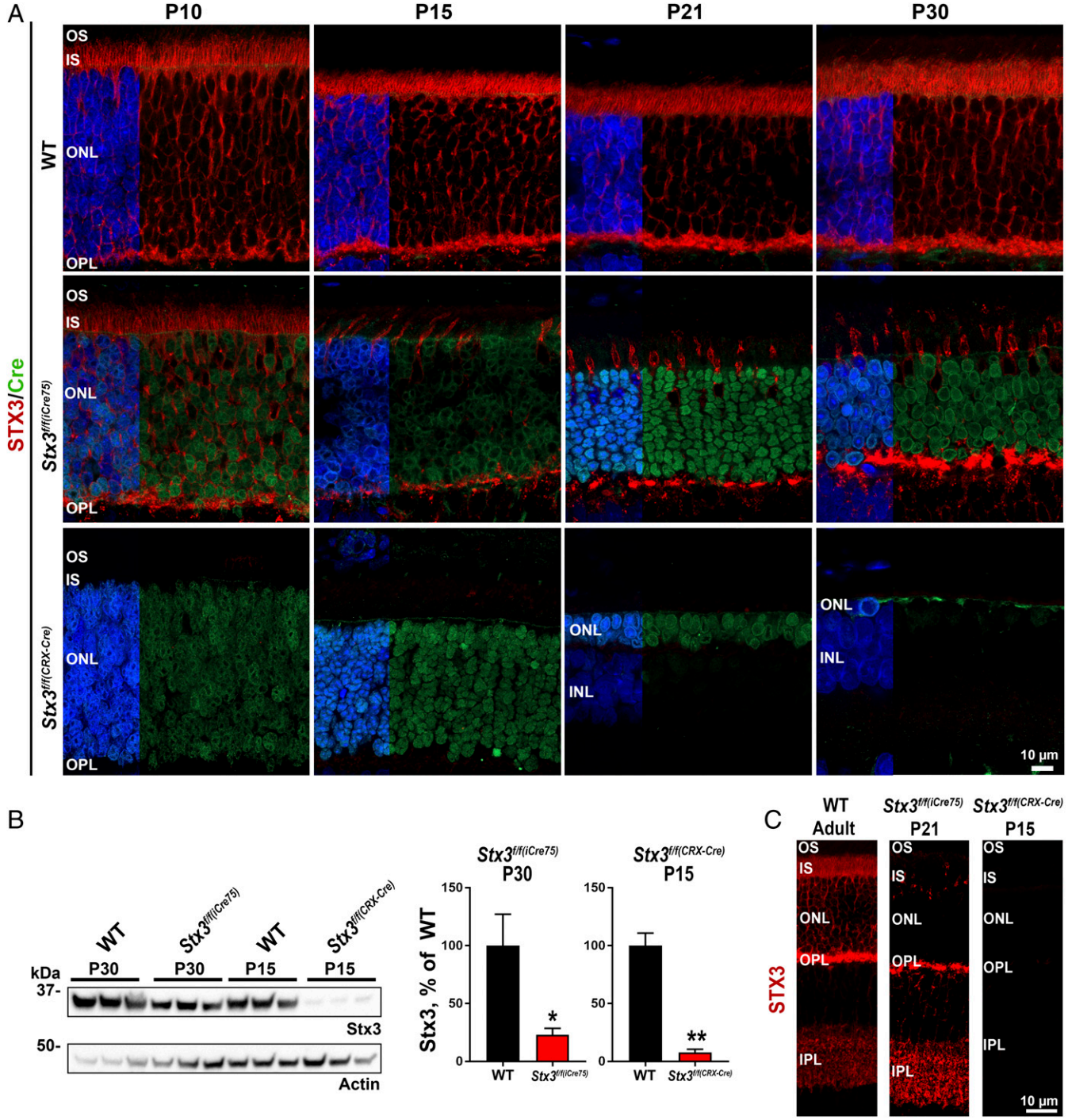

Fig. 1. Conditional knockout of *Stx3* eliminates STX3 expression in photoreceptors. (*A*) Retinal sections were immunofluorescently labeled for STX3 (red), Cre (green), and nuclei (blue). (*B*) STX3 protein levels in $Stx3^{f/f(iCre75)}$ (P30) and $Stx3^{f/f(CRX\text{-}Cre)}$ (P15) retinas were assessed and plotted. Values are mean ± SEM of $n = 3$ independent samples. $^{*}P < 0.05$, $^{**}P < 0.01$ by unpaired two-tailed Student's *t* test. (*C*) Retinal sections were labeled for STX3 (red). (Scale bars: 10 μm in *A* and *C*.)

PRPH2, ROM1, and rhodopsin mislocalized away from the OS to the IS, cell body, and synaptic terminals of photoreceptors (arrows, *SI Appendix*, Fig. S6 *A–C* and Fig. 5*A*). Even though rhodopsin and PRPH2 traffic to the OS through separate pathways (15), PRPH2, ROM1, and rhodopsin showed similar patterns of mislocalization in the $Stx3^{f/f(CRX\text{-}Cre)}$ retina and were largely colocalized (Fig. 5 *A* and *B*, arrowheads, Fig. 5*B*, and *SI Appendix*, Fig. S7, arrows) suggesting they were shunted to a common abnormal location in the absence of STX3. This observation suggests the possibility of the presence of an alternative pathway that could be a default one that uses multiple SNARE complexes and multiple redundancies to get these proteins to their destination. ROM1 showed less mislocalization than PRPH2 or rhodopsin, but mislocalized ROM1 was found in the same punctae as PRPH2 and rhodopsin. Cone opsins trafficked properly to the OS in knockdown retinas (*SI Appendix*, Fig. S6*D*).

RPGR, which is restricted to the base of the connecting cilium and the IS, did not colocalize with mislocalized PRPH2

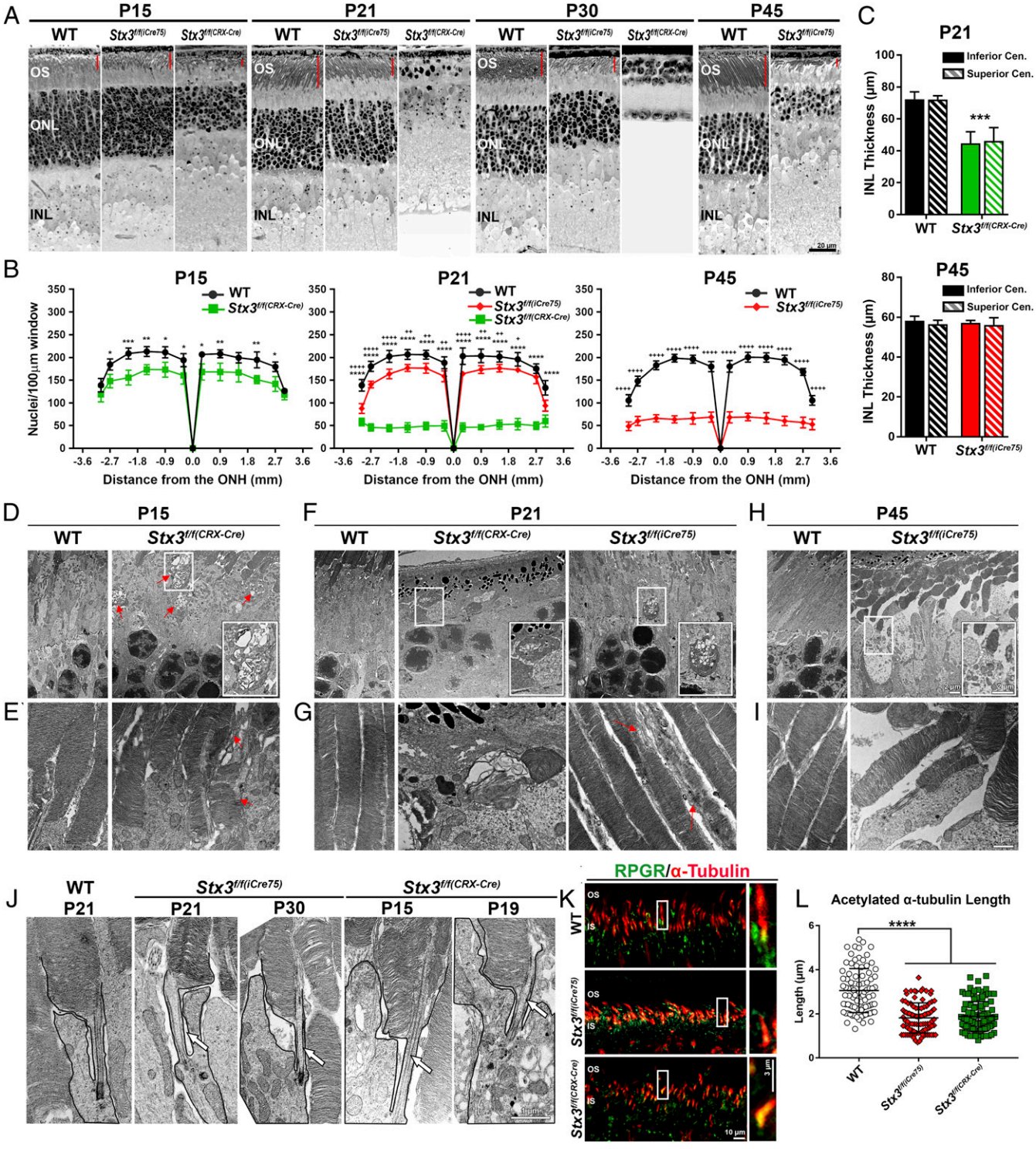

Fig. 2. Elimination of STX3 leads to photoreceptor degeneration. (*A*) Representative light microscopic images. Red bars highlight OS thickness. (*B*) Nuclei in the ONL were counted along the vertical meridian of the eye from the superior to the inferior pole. Measurements were taken from three mice per genotype and time point and plotted as mean ± SD. + denotes comparisons between WT and Stx3$^{f/f(iCre75)}$ retina; * denotes comparisons between WT and Stx3$^{f/f(CRX\text{-}Cre)}$ retina. One symbol $P < 0.05$, two symbols $P < 0.01$, three symbols $P < 0.001$, four symbols $P < 0.0001$ in two-way ANOVA followed by Tukey's post hoc comparisons. (*C*) INL thickness was measured in the inferior central (solid bars) and superior central retina (hashed bars). $n = 3$ mice per genotype, plotted as mean ± SD (*D*–*J*). TEM was from the indicated ages/genotypes. Arrows highlight IS abnormalities (*D*) and OS abnormalities (*G*). *Insets* are expanded views of regions in black boxes. (*J*) Additional TEM showing ISs and connecting cilia (arrows). Black outlines highlight cell borders around the IS/OS junction. (*K*) Retinal sections from adult (WT), P21 [Stx3$^{f/f(iCre75)}$], and P15 [Stx3$^{f/f(CRX\text{-}Cre)}$] were labeled for RPGR (green) and acetylated α-tubulin (red). (*Right*) Expanded views of white boxed regions. (*L*) Connecting cilia/axonemes were measured based on tubulin labeling from 100 photoreceptors from $n = 3$ mice per genotype for a total of 300 axonemes/genotype at the same ages as in *K*. Plotted is mean ± SD, ****$P < 0.0001$ in one-way ANOVA with Tukey's post hoc comparison. (Scale bars: 20 μm in *A*; 2 μm in *D*, *F*, and *H*; 1 μm in *E*, *G*, *I*, and *J*; 10 μm in *K*; and 3 μm in *K*, *Right*.)

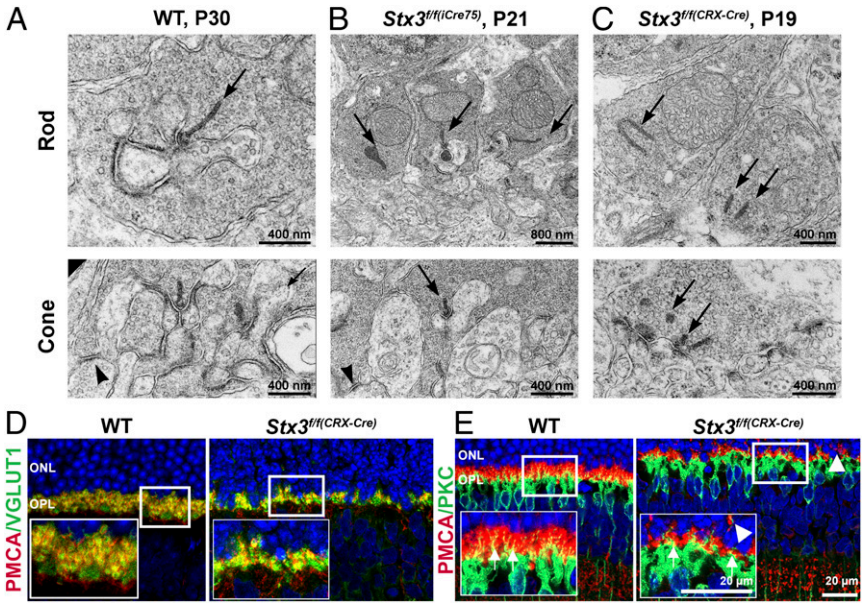

Fig. 3. Conditional knockout of STX3 has deleterious effects on photoreceptor terminal organization. TEM of rod and cone terminals are shown from WT (*A*), *Stx3*$^{f/f(iCre75)}$ (*B*), and *Stx3*$^{f/f(CRX\text{-}Cre)}$ (*C*) retinas. Arrows highlight synaptic ribbons. Arrowheads highlight flat contacts at the base of cone terminals. (*D* and *E*) Retinal sections from P21 WT and P15 *Stx3*$^{f/f(CRX\text{-}Cre)}$ retina were labeled for PMCA (red, photoreceptor and bipolar cell synaptic terminals), and either VGLUT1 (green, photoreceptor and bipolar cell synaptic terminals, *D*) or PKC (green, rod bipolar cells, *E*), and nuclei are blue (DAPI). *Insets* show expanded views of boxed areas. Arrows highlight areas of colocalization where rod bipolar dendrites protrude into rod photoreceptor synapses. Arrowheads show photoreceptor terminals receding into the ONL during degeneration. (Scale bar: 400 nm in *A*–*C*, 800 nm in *B*, and 20 μm in *D* and *E*.)

(*SI Appendix*, Fig. S7*C*, arrowheads) suggesting that mistrafficked OS proteins did not accumulate at the base of the connecting cilium but localized to a different site in the IS. Microtubules move cargo within the cell, and indeed we find that mislocalized PRPH2, ROM1, and rhodopsin in the *Stx3*$^{f/f(CRX\text{-}Cre)}$ colocalize with acetylated α-tubulin within the photoreceptor cell bodies (Fig. 5 *C*–*E*), suggesting that these OS proteins traffic improperly along microtubules to the synaptic terminals in the absence of STX3.

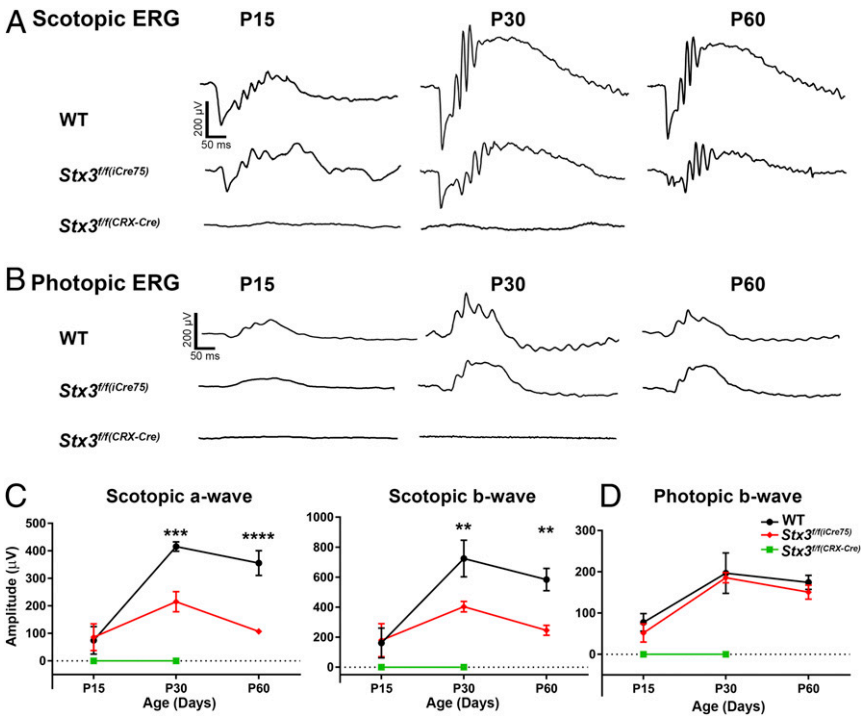

Fig. 4. STX3 knockout impairs photoreceptor function. Full-field scotopic (*A* and *C*) and photopic (*B* and *D*) ERG was performed. (*A* and *B*) Representative ERG waveforms. (*C* and *D*) The amplitude of maximum scotopic a- and b-waves, and maximum photopic b-waves were plotted as mean ± SEM. $n = 3$ to 6 animals for each genotype. $^{**}P < 0.01$, $^{***}P < 0.001$, and $^{****}P < 0.0001$ by two-way ANOVA with Tukey's post hoc comparison.

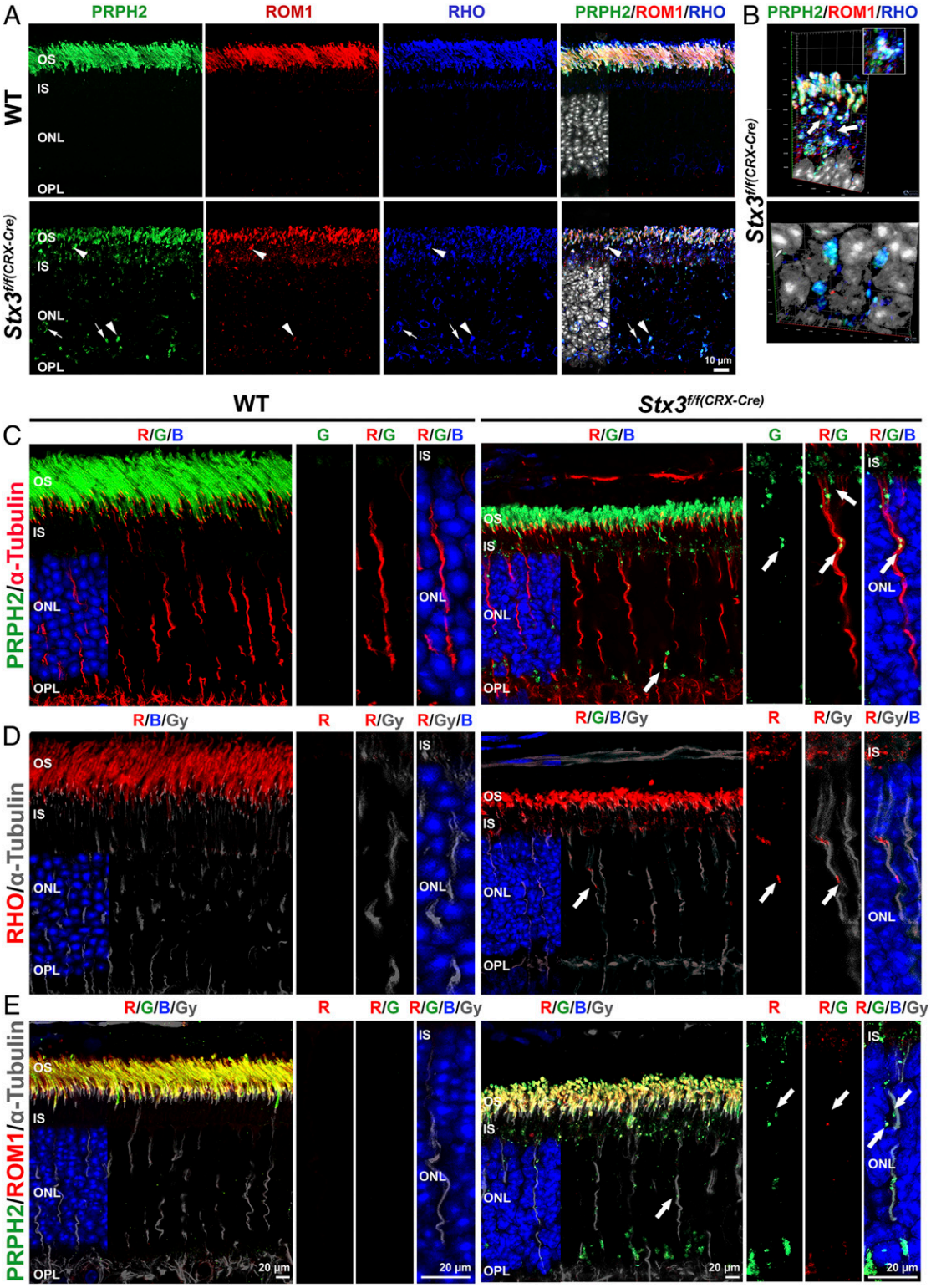

Fig. 5. Mislocalized OS proteins colocalize in the absence of STX3. (*A* and *B*) P15 retinal sections immunolabeled for PRPH2 (green), ROM1 (red), and rhodopsin (RHO, blue). Nuclei are gray (DAPI) in overlay panels. Arrowheads highlight colocalization of all three proteins; arrows show regions where PRPH2/rhodopsin colocalize in the absence of ROM1. (*B*) Three-dimensional reconstructions of confocal stacks (YX planes and YZ planes of 1-μm thickness) highlighting the OSs and ISs (*Top*) or the ONL and OPL (*Bottom*). Arrows highlight regions where all three proteins colocalize. (*C*–*E*) Retinal sections were immunolabeled for PRPH2 (green) and acetylated α-tubulin (red) in *C*; rhodopsin (red) and acetylated α-tubulin (gray) in *D*; and PRPH2 (green), ROM1 (red), and acetylated α-tubulin (gray) in *E*. Nuclei are blue (DAPI). Arrows indicate regions of colocalization. Small panels to the *Right* of each main panel show expanded views of microtubules. Letters above each panel indicate which channels are shown. R, red; G, green; B, blue; Gy, gray. (Scale bars: 10 μm in *A* and 20 μm in *C*–*E*.) For 3D reconstructions, each grid box is 1 μm.

To understand whether mislocalization of OS proteins in *Stx3* knockout was restricted to disc proteins that interact with STX3, we labeled sections from $Stx3^{f/f(CRX\text{-}Cre)}$ retina (which showed more severe defects), with an antibody that recognizes both the rod cyclic nucleotide gated channel (CNGB1) and its nonmembrane bound isoform, glutamic acid rich protein (GARP). CNGB1 and GARP associate with the OS plasma membrane rather than the disc membrane and do not interact with STX3 (17). Critically, CNGB1/GARP did not mislocalize in the $Stx3^{f/f(CRX\text{-}Cre)}$ retina (*SI Appendix*, Fig. S8).

The PRPH2 C Terminus Interacts with SNARE Proteins. Previously we identified STX3, SNAP25, and syntaxin binding protein 1 (STXBP1, also known as munc18) as PRPH2 binding partners (17). As expected, in anti-PRPH2 immunoprecipitations, STX3, SNAP25, and STXBP1 coprecipitated with PRPH2 in WT retinas, but were not pulled down from $Prph2^{-/-}$ retinas (confirming interactions were specific, Fig. 6 *A* and *I*; I, input; FT, flow through; E, bound protein eluted from beads; B, beads with uneluted protein). Both SNAP25 and STXBP1 came down with PRPH2 in $Stx3^{f/f(CRX\text{-}Cre)}$ retinas (Fig. 6*A*), though not to the same extent as in WT, suggesting that STX3 was not essential for interactions between PRPH2 and SNAP25/STXBP1. SNAP25 and STXBP1 are normally part of the SNARE complex at sites of vesicle fusion and are found throughout the IS, cell body, and synaptic terminals (Fig. 6 *B*–*E*). This pattern is altered in the $Stx3^{f/f(CRX\text{-}Cre)}$ retina: instead of even, diffuse labeling in the IS, SNAP25 and STXBP1 colocalized with PRPH2-positive (Fig. 6 *B* and *C*, arrows) and rhodopsin-positive punctae (Fig. 6*D*, arrows) in the IS.

To identify interacting regions of PRPH2 and STX3, we generated GST fusion constructs consisting of GST (control), GST with the cytoplasmic PRPH2 C-terminal (GST-PRPH2-CT), or GST with the STX3 SNARE domain (GST-STX3-SNARE). The PRPH2-CT does not pull down PRPH2 or ROM1 (the second intradiscal loop mediates these interactions) (31). However, GST-PRPH2-CT pulled down STX3, SNAP25, and STXBP1 from WT retinal lysates (lanes 4 and 6, Fig. 6*F*). To confirm that pulldown of STX3/SNAP25/STXBP1 with GST-PRPH2-CT was not due to coprecipitation with full-length PRPH2, we pulled down with GST-PRPH2-CT from the $Prph2^{-/-}$ retina (lane 5, Fig. 6*F*). STX3, STXBP1, and SNAP25 came down with GST-PRPH2-CT, indicating that full-length PRPH2 is not needed for these interactions, and that they are mediated by the PRPH2 C-terminal.

Previously we found that rhodopsin immunoprecipitated from the retina with STX3 antibodies (17). Similarly, rhodopsin also came down with STX3, SNAP25, and STXBP1 in the GST-PRPH2-CT pulldown from WT retina (Fig. 6*F*). Rhodopsin was absent in

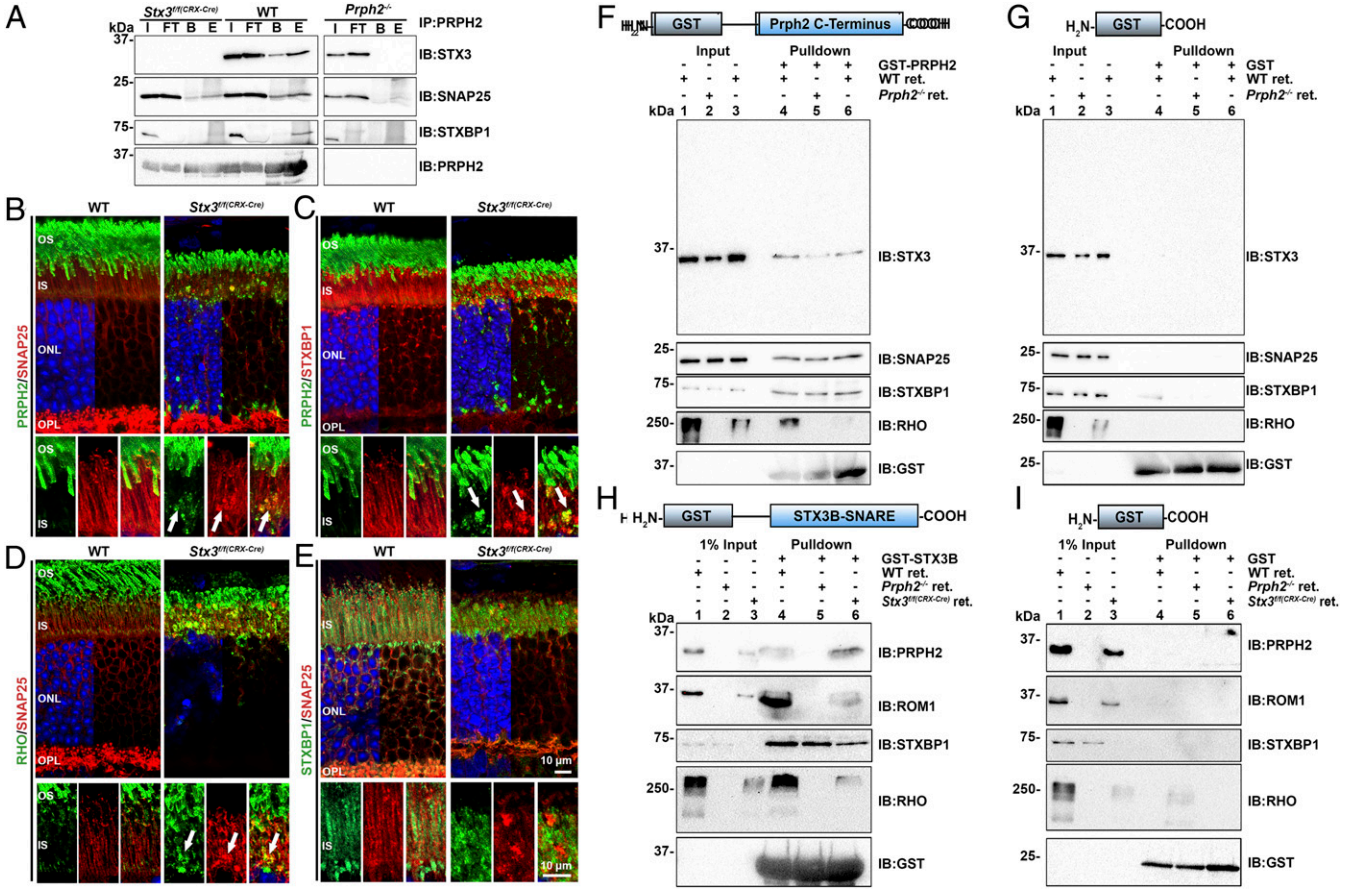

Fig. 6. PRPH2 interacts with SNARE proteins in the absence of STX3. (*A*) Retinal extracts from WT, $Prph2^{-/-}$, and $Stx3^{f/f(CRX\text{-}Cre)}$ mice underwent immunoprecipitation with PRPH2 antibodies (RDS-CT) and blots were probed for STX3, SNAP25, STXBP1, and PRPH2. I, input; FT, flow through (unbound); E, bound fraction eluted from beads; and B, bound fraction on beads. (*B*–*E*) Retinal sections immunolabeled for PRPH2 (green) and SNAP25 (red) in *B*, PRPH2 (green) and STXBP1 (red) in *C*, rhodopsin (RHO, green) and SNAP25 (red) in *D*, and STXBP1 (green) and SNAP25 (red) in *E*. Nuclei are blue (DAPI). Images shown are projection images from confocal microscope (63×). Arrows indicate regions of colocalization. (*F*–*I*) GST fusion constructs were generated, consisting of the PRPH2 C-terminal (*F*), the STX3 SNARE domain (*H*), or GST alone as control (*G* and *I*). GST proteins were incubated with retinal extracts as indicated at the *Top Right* of each panel. Each blot has input (total retinal lysate) on the *Left* and eluents from the GST pulldowns on the *Right*. Rhodopsin is present in large >250-kDa aggregates because the beads are boiled to elute sample, and input samples are prepared the same way to promote consistency. (Scale bars: 10 μm.)

pulldowns from the *Prph2*$^{-/-}$ retina (Fig. 6*F*, lane 5), likely reflecting the fact that rhodopsin levels are undetectably low in the *Prph2*$^{-/-}$ (Fig. 6*F*, lane 2). No STX3, SNAP25, or rhodopsin were pulled down with the negative control (GST, Fig. 6*G*). To identify the region of STX3 involved in interactions with PRPH2, complexes pulled down by the STX3 SNARE domain were evaluated (Fig. 6 *H* and *I*). GST-STX3-SNARE pulled down PRPH2, ROM1, STXBP1, and rhodopsin from WT retina (Fig. 6*H*, lane 4). These four proteins were also pulled down with GST-STX3-SNARE from *Stx3*$^{f/f(CRX\text{-}Cre)}$ retinas (Fig. 6*H*, lane 6), confirming that full-length STX3 was not needed for these interactions to occur, rather they are mediated directly or indirectly by the STX3 SNARE domain. ROM1 and rhodopsin were not pulled down from the *Prph2*$^{-/-}$ retina, but again, these proteins are virtually undetectable in the absence of *Prph2*$^{-/-}$.

Discussion

Here we present evidence supporting the importance of STX3 for photoreceptor OS protein trafficking and health. Knockout of STX3 in photoreceptors leads to early-onset, rapid degeneration. In the absence of STX3, photoreceptors exhibit defects in both the IS/OS where STX3 is involved in protein targeting to the OS, and at the synaptic terminals where STX3 is essential for proper synaptic vesicle release. Critically, in the absence of STX3 in rods, photoreceptor disc proteins such as PRPH2, ROM1, and rhodopsin mislocalize, as do vesicle fusion components STXBP1 and SNAP25, while OS plasma membrane proteins such as CNGB1/GARP do not. Given our observation that PRPH2, ROM1, and rhodopsin (but not CNGB1/GARP) interact with STX3 and other SNAREs such as SNAP25, and regulators of SNARE function, such as STXBP1, these findings suggest that STX3-mediated vesicle fusion is critical for proper delivery of disc proteins to the OS.

One interesting finding is that cone opsins traffic to the OS normally in the absence of STX3, while mislocalized PRPH2 colocalizes with mislocalized rhodopsin, suggesting that PRPH2 in cones was not mistrafficked. These observations suggest that cones traffic OS proteins differently from rods, an idea that is supported by other literature (32, 33). For example, mutations that affect PRPH2 oligomerization lead to mislocalization of PRPH2 and cone opsins, but do not affect rhodopsin trafficking (34, 35). These differences in rod vs. cone trafficking pathways may be part of the mechanism which leads to differences in OS assembly in rod vs. cone. We have previously found that in rods, disc formation is not initiated without PRPH2, while cone OS lamellae evaginate as long as cone opsins are present, with PRPH2 being important for disc rim formation as a second step (36–38). However, the linkage between differences in OS protein targeting and differences in OS assembly in rods vs. cones (as well as pathways for cone OS targeting) is an area where further exploration is needed.

Rhodopsin trafficking relies on small GTPases (Rab11, Rab8, and Arf4) and associated regulators (reviewed in refs. 39 and 40), STX3, SNAP25, VAMP7 (20, 41), and the Smad Anchor for Receptor Activation (SARA) (42), another STX3 interacting partner. SARA is important for vesicle fusion at early endosomes, and rhodopsin mislocalizes when SARA levels are reduced (42). Our understanding of PRPH2 trafficking lags significantly behind our understanding of rhodopsin trafficking, and no critical targeting GTPases have yet been identified. A significant amount of PRPH2 traffics via an unconventional route that bypasses the trans-Golgi (16, 17), but the molecular regulators of this pathway remain unknown. Recently, a role for Rab11a and late endosomes in PRPH2 ciliary/OS targeting has been proposed (19). Although these data may fit with our findings, there is no solid evidence that late endosomes are involved in the trafficking of OS membrane proteins in vertebrate rods. For such a system to exist, those proteins have to be delivered to the plasma membrane first, then endocytosed through early endosomes into the recycling endosome. The absence of such a system is supported by the lack of OS proteins in the IS plasma membrane in our study.

Despite the mislocalization of PRPH2, rhodopsin, and ROM1 in the absence of STX3, it is worth noting that a substantial fraction of these proteins is still delivered to the OS. It is possible that other syntaxins not usually expressed in photoreceptors are up-regulated in the *Stx3* knockouts or that other alternative pathways exist that are syntaxin-independent mechanisms to deliver membrane proteins to the OS. It is known that proteins lacking specific targeting signals for other cellular compartments can be delivered to the OS by default (43). Much remains to be understood about how OS proteins are delivered to the OS.

An exciting finding is that interactions between PRPH2, STX3, SNAP25, and STXBP1 are mediated by the C-terminal of PRPH2 and the SNARE domain of STX3. The PRPH2 C-terminal is an attractive candidate interaction domain. It consists of amphipathic alpha-helices and intrinsically disordered domains, is known to interact with other proteins, and promotes OS targeting, disc curvature, and membrane fusion (11, 12, 44–48). Our data support the previously proposed hypothesis that the PRPH2 C-terminal may take the place of the v-SNARE in vesicle fusion during OS targeting (46, 49, 50). However, it is also possible that PRPH2 is an essential regulator of membrane fusion, but does not itself directly participate in a membrane fusion complex. In this case, the putative v-SNARE could be VAMP7, which has been shown in a frog model to be a v-SNARE involved in targeting rhodopsin vesicles (41). There is also support for tetraspanins (like PRPH2) to play a critical regulatory role with VAMP7 in other systems. For example, the tetraspanin protein CD82 regulates clathrin-mediated endocytosis of epidermal growth factor receptor (EGFR), and delivery of CD82 to the cell surface is dependent on VAMP7 (51). Clathrin vesicles are a part of STX3-mediated photoreceptor trafficking pathways (52) and, given the emerging importance of endosomal pathways in the trafficking of PRPH2 (19), this represents an exciting area for future exploration.

Retinal degeneration in *Stx3* knockouts was severe and rapid. Photoreceptor death often follows malformation of OSs, (e.g., *Rho*$^{-/-}$ and *Prph2*$^{-/-}$), so defects in OS protein trafficking and abnormal OS structure may contribute to photoreceptor degeneration in the *Stx3* knockouts. However, degeneration in both *Stx3* knockout lines was more rapid than in either the *Rho*$^{-/-}$ or *Prph2*$^{-/-}$ (10, 53), suggesting other mechanisms, such as synaptic dysfunction, also contribute to the degeneration. In addition to its role in OS protein trafficking, STX3 is essential for synaptic vesicle exocytosis/release in photoreceptors (23, 54). Consistent with a role for STX3 in synaptic release, we find that *Stx3* knockout rod and cone synapses are highly abnormal. In addition to synaptic defects arising due to impaired synaptic vesicle release (i.e., direct consequences of STX3 loss in synaptic terminals), the terminals may suffer additional effects from STX3 loss. Many rod terminals in *Stx3*$^{f/f(CRX\text{-}Cre)}$ retinas accumulate abnormal membranous vacuoles/vesicles. This accumulation of membranous material may represent mistrafficked PRPH2/rhodopsin or disruption of normal synaptic vesicle cycling mechanisms, and thus contribute to accelerated degeneration.

Understanding the differences in photoreceptor protein sorting and trafficking mechanisms for different photoreceptor compartments and subcompartments is an essential unanswered cell biological question. Our studies provide strong evidence that STX3 is an essential piece of the trafficking puzzle and is critical for photoreceptor health. Critically, our findings suggest that cones and rods rely on different trafficking components, a finding which has significant implications for their differing OS structure. In addition, our data suggest that though initially trafficked separately, OS disc membrane and disc rim (but not OS plasma membrane) components converge at a STX3-dependent fusion

event, providing increased mechanistic understanding for how proteins are sorted during OS biogenesis. These studies significantly expand our understanding of this process and open up several exciting areas for future exploration.

Materials and Methods

Additional information for each section is in *SI Appendix*.

Animals. Animal experiments were approved by the University of Houston Institutional Animal Care and Use Committee and adhered to recommendations in the NIH Guide for the Care and Use of Laboratory Animals. *Stx3* flox/flox (*Stx3*$^{f/f}$) mice were generated by inGenious Targeting Laboratory, Inc., Ronkonkoma, NY and crossed with *iCre75* transgenic mice (generated by Ching-Kang Chen, Baylor College of Medicine, Houston TX and made available with permission by Wolfgang Baehr, University of Utah, Salt Lake City, UT) (26) or *CRX-Cre* transgenic mice (generated by Tom M. Glaser, University of California, Davis, CA and made available with permission by Anand Swaroop, National Eye Institute, NIH, Bethesda, MD).

Immunofluorescence, Immunoblotting, Immunoprecipitation, and GST Pulldown. Immunofluorescence, immunoprecipitation, SDS/PAGE, and Western blotting using retinal extracts were performed as described previously (17, 35, 55). GST pulldowns were performed as described previously using GST-STX3-SNARE (generously provided by Roger Janz, McGovern Medical School, UTHealth, Houston, TX) (56), GST-PRPH2-CT (31), and GST (expressed from pGEX4T2). Details on antibodies used are provided in *SI Appendix*, Table S1.

Electroretinography. Full-field dark-adapted and light-adapted ERGs were recorded as previously described (57).

Transmission Electron Microscopy and Light Microscopic Histology. Methods used for tissue collection, processing, plastic embedding, and TEM were described previously (35, 36, 58).

Statistical Analysis. Statistical testing was performed using GraphPad Prism, v.8.3.0 (GraphPad Software) and post hoc testing in cases with multiple groups was employed. All experiments (e.g., IF labeling, GST pulldown, ERG) were done on at least three separate occasions regardless of the number of individual animals used for each study.

Data Availability. All data are included in the manuscript and *SI Appendix*.

ACKNOWLEDGMENTS. We thank Drs. Ching-Kang Chen, Wolfgang Baehr, Tom M. Glaser, Anand Swaroop, Hemant Khanna, Vadim Arshavsky, Roger Janz, and Robert Molday for the provision of tools as indicated in the text. This work was supported by the NIH (R01EY10609 to M.I.N. and M.R.A.-U., and National Institute of General Medical Sciences 1 P20 GM12552801A1 to S.M.C.).

1. R. W. Young, The renewal of photoreceptor cell outer segments. *J. Cell Biol.* **33**, 61–72 (1967).
2. R. W. Young, D. Bok, Participation of the retinal pigment epithelium in the rod outer segment renewal process. *J. Cell Biol.* **42**, 392–403 (1969).
3. T. Burgoyne *et al*., Rod disc renewal occurs by evagination of the ciliary plasma membrane that makes cadherin-based contacts with the inner segment. *Proc. Natl. Acad. Sci. U.S.A.* **112**, 15922–15927 (2015).
4. J. D. Ding, R. Y. Salinas, V. Y. Arshavsky, Discs of mammalian rod photoreceptors form through the membrane evagination mechanism. *J. Cell Biol.* **211**, 495–502 (2015).
5. R. H. Steinberg, S. K. Fisher, D. H. Anderson, Disc morphogenesis in vertebrate photoreceptors. *J. Comp. Neurol.* **190**, 501–508 (1980).
6. S. Volland *et al*., Three-dimensional organization of nascent rod outer segment disk membranes. *Proc. Natl. Acad. Sci. U.S.A.* **112**, 14870–14875 (2015).
7. M. L. Milstein *et al*., Multistep peripherin-2/rds self-assembly drives membrane curvature for outer segment disk architecture and photoreceptor viability. *Proc. Natl. Acad. Sci. U.S.A.* **117**, 4400–4410 (2020).
8. K. Arikawa, L. L. Molday, R. S. Molday, D. S. Williams, Localization of peripherin/rds in the disk membranes of cone and rod photoreceptors: Relationship to disk membrane morphogenesis and retinal degeneration. *J. Cell Biol.* **116**, 659–667 (1992).
9. C. J. Boon *et al*., The spectrum of retinal dystrophies caused by mutations in the peripherin/RDS gene. *Prog. Retin. Eye Res.* **27**, 213–235 (2008).
10. S. Sanyal, A. De Ruiter, R. K. Hawkins, Development and degeneration of retina in rds mutant mice: Light microscopy. *J. Comp. Neurol.* **194**, 193–207 (1980).
11. B. M. Tam, O. L. Moritz, D. S. Papermaster, The C terminus of peripherin/rds participates in rod outer segment targeting and alignment of disk incisures. *Mol. Biol. Cell* **15**, 2027–2037 (2004).
12. R. Y. Salinas, S. A. Baker, S. M. Gospe 3rd, V. Y. Arshavsky, A single valine residue plays an essential role in peripherin/rds targeting to photoreceptor outer segments. *PLoS One* **8**, e54292 (2013).
13. P. Avasthi *et al*., Trafficking of membrane proteins to cone but not rod outer segments is dependent on heterotrimeric kinesin-II. *J. Neurosci.* **29**, 14287–14298 (2009).
14. M. M. Abd-El-Barr *et al*., Impaired photoreceptor protein transport and synaptic transmission in a mouse model of Bardet-Biedl syndrome. *Vision Res.* **47**, 3394–3407 (2007).
15. R. N. Fariss, R. S. Molday, S. K. Fisher, B. Matsumoto, Evidence from normal and degenerating photoreceptors that two outer segment integral membrane proteins have separate transport pathways. *J. Comp. Neurol.* **387**, 148–156 (1997).
16. G. Tian *et al*., An unconventional secretory pathway mediates the cilia targeting of peripherin/rds. *J. Neurosci.* **34**, 992–1006 (2014).
17. R. Zulliger *et al*., SNAREs interact with retinal degeneration slow and rod outer segment membrane protein-1 during conventional and unconventional outer segment targeting. *PLoS One* **10**, e0138508 (2015).
18. S. M. Conley *et al*., Prph2 initiates outer segment morphogenesis but maturation requires Prph2/Rom1 oligomerization. *Hum. Mol. Genet.* **28**, 459–475 (2019).
19. W. Otsu, Y. C. Hsu, J. Z. Chuang, C. H. Sung, The late endosomal pathway regulates the ciliary targeting of tetraspanin protein peripherin 2. *J. Neurosci.* **39**, 3376–3393 (2019).
20. J. Mazelova, N. Ransom, L. Astuto-Gribble, M. C. Wilson, D. Deretic, Syntaxin 3 and SNAP-25 pairing, regulated by omega-3 docosahexaenoic acid, controls the delivery of rhodopsin for the biogenesis of cilia-derived sensory organelles, the rod outer segments. *J. Cell Sci.* **122**, 2003–2013 (2009).
21. E. Sanchez *et al*., Syntaxin 3, but not syntaxin 4, is required for mast cell-regulated exocytosis, where it plays a primary role mediating compound exocytosis. *J. Biol. Chem.* **294**, 3012–3023 (2019).
22. L. Curtis *et al*., Syntaxin 3B is essential for the exocytosis of synaptic vesicles in ribbon synapses of the retina. *Neuroscience* **166**, 832–841 (2010).
23. D. M. Sherry, R. Mitchell, K. M. Standifer, B. du Plessis, Distribution of plasma membrane-associated syntaxins 1 through 4 indicates distinct trafficking functions in the synaptic layers of the mouse retina. *BMC Neurosci.* **7**, 54 (2006).
24. A. Nishida *et al*., Otx2 homeobox gene controls retinal photoreceptor cell fate and pineal gland development. *Nat. Neurosci.* **6**, 1255–1263 (2003).
25. L. Prasov, T. Glaser, Pushing the envelope of retinal ganglion cell genesis: Context dependent function of Math5 (Atoh7). *Dev. Biol.* **368**, 214–230 (2012).
26. S. Li *et al*., Rhodopsin-iCre transgenic mouse line for Cre-mediated rod-specific gene targeting. *Genesis* **41**, 73–80 (2005).
27. A. Furukawa, C. Koike, P. Lippincott, C. L. Cepko, T. Furukawa, The mouse Crx 5′-upstream transgene sequence directs cell-specific and developmentally regulated expression in retinal photoreceptor cells. *J. Neurosci.* **22**, 1640–1647 (2002).
28. T. Furukawa, E. M. Morrow, C. L. Cepko, Crx, a novel otx-like homeobox gene, shows photoreceptor-specific expression and regulates photoreceptor differentiation. *Cell* **91**, 531–541 (1997).
29. J. Johnson *et al*., Vesicular glutamate transporter 3 (VGLUT3) expression identifies glutamatergic amacrine cells in the rodent retina. *J. Comp. Neurol.* **477**, 386–398 (2004).
30. J. E. Johnson Jr. *et al*., Spatiotemporal regulation of ATP and Ca2+ dynamics in vertebrate rod and cone ribbon synapses. *Mol. Vis.* **13**, 887–919 (2007).
31. X. Q. Ding, H. M. Stricker, M. I. Naash, Role of the second intradiscal loop of peripherin/rds in homo and hetero associations. *Biochemistry* **44**, 4897–4904 (2005).
32. S. Karan, H. Zhang, S. Li, J. M. Frederick, W. Baehr, A model for transport of membrane-associated phototransduction polypeptides in rod and cone photoreceptor inner segments. *Vision Res.* **48**, 442–452 (2008).
33. R. K. Raghupathy *et al*., Rpgrip1 is required for rod outer segment development and ciliary protein trafficking in zebrafish. *Sci. Rep.* **7**, 16881 (2017).
34. S. M. Conley, D. Chakraborty, M. I. Naash, Mislocalization of oligomerization-incompetent RDS is associated with mislocalization of cone opsins and cone transducin. *Adv. Exp. Med. Biol.* **723**, 657–662 (2012).
35. D. Chakraborty, X. Q. Ding, S. M. Conley, S. J. Fliesler, M. I. Naash, Differential requirements for retinal degeneration slow intermolecular disulfide-linked oligomerization in rods versus cones. *Hum. Mol. Genet.* **18**, 797–808 (2009).
36. R. Farjo *et al*., Retention of function without normal disc morphogenesis occurs in cone but not rod photoreceptors. *J. Cell Biol.* **173**, 59–68 (2006).
37. S. M. Conley *et al*., Insights into the mechanisms of macular degeneration associated with the R172W mutation in RDS. *Hum. Mol. Genet.* **23**, 3102–3114 (2014).
38. D. Chakraborty, S. M. Conley, M. R. Al-Ubaidi, M. I. Naash, Initiation of rod outer segment disc formation requires RDS. *PLoS One* **9**, e98939 (2014).
39. J. Wang, D. Deretic, Molecular complexes that direct rhodopsin transport to primary cilia. *Prog. Retin. Eye Res.* **38**, 1–19 (2014).
40. J. N. Pearring, R. Y. Salinas, S. A. Baker, V. Y. Arshavsky, Protein sorting, targeting and trafficking in photoreceptor cells. *Prog. Retin. Eye Res.* **36**, 24–51 (2013).
41. V. Kandachar, B. M. Tam, O. L. Moritz, D. Deretic, An interaction network between the SNARE VAMP7 and Rab GTPases within a ciliary membrane-targeting complex. *J. Cell Sci.* **131**, jcs222034 (2018).
42. J. Z. Chuang, Y. Zhao, C. H. Sung, SARA-regulated vesicular targeting underlies formation of the light-sensing organelle in mammalian rods. *Cell* **130**, 535–547 (2007).
43. S. A. Baker *et al*., The outer segment serves as a default destination for the trafficking of membrane proteins in photoreceptors. *J. Cell Biol.* **183**, 485–498 (2008).

44. M. L. Milstein, V. A. Kimler, C. Ghatak, A. S. Ladokhin, A. F. X. Goldberg, An inducible amphipathic helix within the intrinsically disordered C terminus can participate in membrane curvature generation by peripherin-2/rds. *J. Biol. Chem.* **292**, 7850–7865 (2017).
45. N. Khattree, L. M. Ritter, A. F. Goldberg, Membrane curvature generation by a C-terminal amphipathic helix in peripherin-2/rds, a tetraspanin required for photoreceptor sensory cilium morphogenesis. *J. Cell Sci.* **126**, 4659–4670 (2013).
46. K. Boesze-Battaglia *et al*., The tetraspanin protein peripherin-2 forms a complex with melanoregulin, a putative membrane fusion regulator. *Biochemistry* **46**, 1256–1272 (2007).
47. M. Damek-Poprawa, J. Krouse, C. Gretzula, K. Boesze-Battaglia, A novel tetraspanin fusion protein, peripherin-2, requires a region upstream of the fusion domain for activity. *J. Biol. Chem.* **280**, 9217–9224 (2005).
48. T. C. Edrington 5th, P. L. Yeagle, C. L. Gretzula, K. Boesze-Battaglia, Calcium-dependent association of calmodulin with the C-terminal domain of the tetraspanin protein peripherin/rds. *Biochemistry* **46**, 3862–3871 (2007).
49. K. Boesze-Battagliaa, F. P. Stefano, Peripherin/rds fusogenic function correlates with subunit assembly. *Exp. Eye Res.* **75**, 227–231 (2002).
50. K. Boesze-Battaglia, O. P. Lamba, A. A. Napoli Jr., S. Sinha, Y. Guo, Fusion between retinal rod outer segment membranes and model membranes: A role for photoreceptor peripherin/rds. *Biochemistry* **37**, 9477–9487 (1998).
51. M. Chaineau, L. Danglot, T. Galli, Multiple roles of the vesicular-SNARE TI-VAMP in post-Golgi and endosomal trafficking. *FEBS Lett.* **583**, 3817–3826 (2009).
52. S. Veleri *et al*., REEP6 mediates trafficking of a subset of Clathrin-coated vesicles and is critical for rod photoreceptor function and survival. *Hum. Mol. Genet.* **26**, 2218–2230 (2017).
53. J. Lem *et al*., Morphological, physiological, and biochemical changes in rhodopsin knockout mice. *Proc. Natl. Acad. Sci. U.S.A.* **96**, 736–741 (1999).
54. C. L. Hays *et al*., Simultaneous release of multiple vesicles from rods involves synaptic ribbons and syntaxin 3B. *Biophys. J.* **118**, 967–979 (2020).
55. M. W. Stuck, S. M. Conley, M. I. Naash, The Y141C knockin mutation in RDS leads to complex phenotypes in the mouse. *Hum. Mol. Genet.* **23**, 6260–6274 (2014).
56. X. Liu, R. Heidelberger, R. Janz, Phosphorylation of syntaxin 3B by CaMKII regulates the formation of t-SNARE complexes. *Mol. Cell. Neurosci.* **60**, 53–62 (2014).
57. W. L. Cheng, Z. F. Qian, J. Su, [Effect of huoxue tablet on the rheology of erythrocyte in primary hypertension]. *Zhongguo Zhong Xi Yi Jie He Za Zhi* **17**, 718–720 (1997).
58. H. M. Stricker, X.-Q. Ding, A. Quiambao, S. J. Fliesler, M. I. Naash, The Cys214–>Ser mutation in peripherin/rds causes a loss-of-function phenotype in transgenic mice. *Biochem. J.* **388**, 605–613 (2005).